Measurement of the f_+ form factor in $K^0_L \to \pi^\pm e^\mp \nu$ decays using a large hydrogen bubble chamber

A. Engler, G. S. Keyes,* R. W. Kraemer, and M. Tanaka†
Carnegie-Mellon University, Pittsburgh, Pennsylvania 15213

Y. Cho, M. Derrick, D. Lissauer,‡ R. J. Miller, and J. Schlereth
Argonne National Laboratory, Argonne, Illinois 60439

(Received 14 February 1978)

The decay $K^0_L \to \pi e \nu$ was studied in an experiment using the Argonne 12-ft bubble chamber exposed to a K^0_L beam of momentum 550 ± 35 MeV/c. Use of the monochromatic beam and the large chamber volume allowed the selection of about 12000 K^0_{e3} events, containing a small [$(5.3 \pm 0.5)\%$] and well understood background from $K^0_{\mu 3}$ decay. The main feature of this experiment is the good acceptance over the Dalitz plot which minimizes possible systematic errors in the determination of the vector form factor $f_+(q^2)$. We find that the data are adequately described by a linear q^2 parameterization, $f_+(q^2) = f_+(0)[1 + \lambda_+ q^2/m_\pi^2]$, with the slope parameter $\lambda_+ = 0.028 \pm 0.004$ before radiative corrections are made. Direct application of radiative corrections, as calculated by Ginsberg, yields $\lambda_+ = 0.025 \pm 0.005$. Our result is in good agreement with other recent experiments and with the assumption of $K^*(890)$ dominance.

I. INTRODUCTION

The transition matrix element for K-meson semileptonic decay K_{l3} is written as a product of a strangeness-changing weak hadronic current and a leptonic current,

$$M = \frac{G}{\sqrt{2}} \sin\theta_C \langle \pi | J_\mu^{\Delta S=1} | K \rangle \langle l | j_\mu | \nu \rangle , \tag{1}$$

where G is the Fermi constant and θ_C is the Cabibbo angle. It is well established[1] that K_{l3} decay is a vector transition and thus Eq. (1) can be written as

$$M = \frac{G}{\sqrt{2}} \sin\theta_C [f_+(q^2)(P_K + P_\pi)^\mu \bar{u}_l \gamma_\mu (1+\gamma_5) u_\nu + f_-(q^2)(P_K - P_\pi)^\mu \bar{u}_l \gamma_\mu (1+\gamma_5) u_\nu] . \tag{2}$$

The only unknown parts of the interaction are the form factors f_+ and f_- which, assuming time-reversal invariance, are real functions of q^2 only. In the K rest frame, q^2 is given by

$$q^2 = (m_K - m_\pi)^2 - 2 m_K T_\pi^* , \tag{3}$$

where T_π^* is the kinetic energy of the pion.

When the transition rate is calculated from Eq. (2), the terms involving f_- are seen to be multiplied by a factor m_l^2/m_K^2 relative to the f_+ terms. Therefore only f_+ is involved in the K_{e3} transition. This form factor can be expanded in a Taylor series in q^2/m_π^2,

$$f_+(q^2) = f_+(0)[1 + \lambda_+ q^2/m_\pi^2 + \cdots] . \tag{4}$$

The scale for the expansion coefficients can be set by assuming that the vector $K\pi$ interaction is dominated by the $K^*(890)$. This gives

$$f_+(q^2) = f_+(0) M_{K^*}^2/(M_{K^*}^2 - q^2) . \tag{5}$$

Expanding in $q^2/M_{K^*}^2$ and comparing to (4) leads to

$$\lambda_+ = m_\pi^2/m_{K^*}^2 = 0.025 . \tag{6}$$

Thus K^* dominance implies that $f_+(q^2)$ is, to good accuracy, linear in q^2. Since the decays K^+_{e3} and K^0_{e3} are related by the $\Delta I = \frac{1}{2}$ rule, independent information on f_+ can be obtained from K^+_{e3}. Finally, f_+ can also be measured in $K_{\mu 3}$ decay.

Many experiments[2] have measured the form factor f_+ using beams of charged or neutral K mesons. In the decay of charged K mesons one faces the difficulty of detecting the π^0 and measuring its energy. In K^0_L decay experiments, the beam momentum is usually not known and the kinematics then give two different solutions for the K^0_L momentum and hence a two-fold ambiguity for the location of an event on the Dalitz plot. Since λ_+ is expected to be small, the form factor will cause only a minor modulation of the distribution of events on the Dalitz plot. Therefore it is crucial to know the detection efficiency and background across the Dalitz plot, particularly in the pion energy variable T_π^*.

The early experiments on K^0_L decay suffered from poor statistical accuracy or low detection efficiency with consequent large corrections. Recently, results from two very high-statistics spark-chamber experiments were reported, one on $K^0_{\mu 3}$ (Ref. 3) and one on K^0_{e3} (Ref. 4). The large

data sample of these experiments permit rather detailed checks for possible systematic effects. However, the analyses of these experiments rely on very accurate Monte Carlo simulations and their final precision is limited by systematic errors. We have carried out an experiment using a large bubble chamber filled with hydrogen and exposed to a low momentum, monochromatic K_L^0 beam. The use of the monochromatic beam avoids the two-fold kinematic ambiguity. Furthermore, due to the large chamber volume and the low beam momentum, we achieve a high and essentially uniform detection efficiency across the Dalitz plot. The bubble chamber also allows the simultaneous study of both semileptonic decays, K_{e3}^0 and $K_{\mu 3}^0$, and therefore provides independent determinations of the form factors within one experiment. The present paper gives the results of our analysis of the K_{e3}^0 channel. As we shall show, our result depends only weakly on the details of Monte Carlo simulations and is essentially free of systematic errors.

II. EXPERIMENTAL PROCEDURE

The K_L^0 beam to the ANL 12-ft bubble chamber was produced by a 1.03 GeV/c π^- beam focused on a 6-ft-long liquid hydrogen target.[5] Figure 1 shows, schematically, the relationship between the H_2 target, the K_L^0 window, and the bubble chamber. The fiducial volume was chosen to match the acceptance defined by the window. The angles of the K_L^0, determined by the location of the event in the chamber and the measured π^- beam profile, are known to about 15 mr in azimuth, θ, and 10 mr in the dip, λ. In addition, since the only K^0 production channel open at this energy is $\pi^- p \to K^0 \Lambda$, the window defines a nearly monochromatic beam ($\pm$ 35 MeV/c) as shown in Fig. 2.

Approximately 300 000 pictures were scanned for V^0 events and about one-third of the film was double-scanned. We have determined the single-scan efficiency for finding three-body decays to be $(88 \pm 1)\%$.

A significant fraction of the tracks resulting from K_L^0 decay can be identified visually. Electrons which show characteristic spirals, or pions which come to rest or interact, or μ mesons which come to rest and decay, were all recorded during scanning. Events were measured using image plane digitizers attached to the scanning tables and were reconstructed in space using the program TVGP. Tracks which left the bubble chamber without interacting or decaying were measured in two segments: one which originated at the vee vertex and the other terminating at the end of the track. For each mass hypothesis, the measured variables (θ, λ, p) of the first segment were extrapolated from the vee vertex to the beginning point of the second segment taking into account energy loss and the magnetic field shape. The track was classified as an electron if the total track length measured in this way, assuming

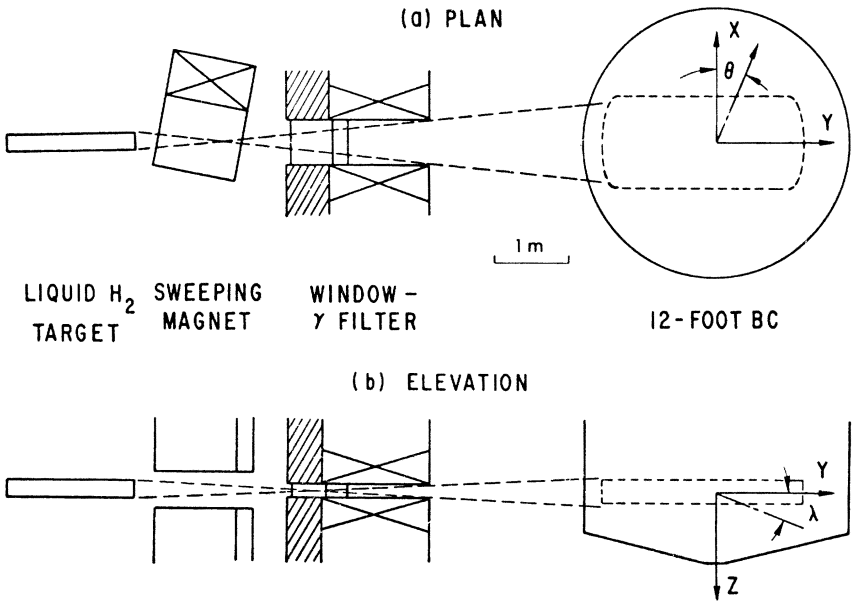

FIG. 1. End section of the beam, showing schematically the relationship between the target, the K_L^0 window, and the bubble chamber. The chamber fiducial volume is also indicated.

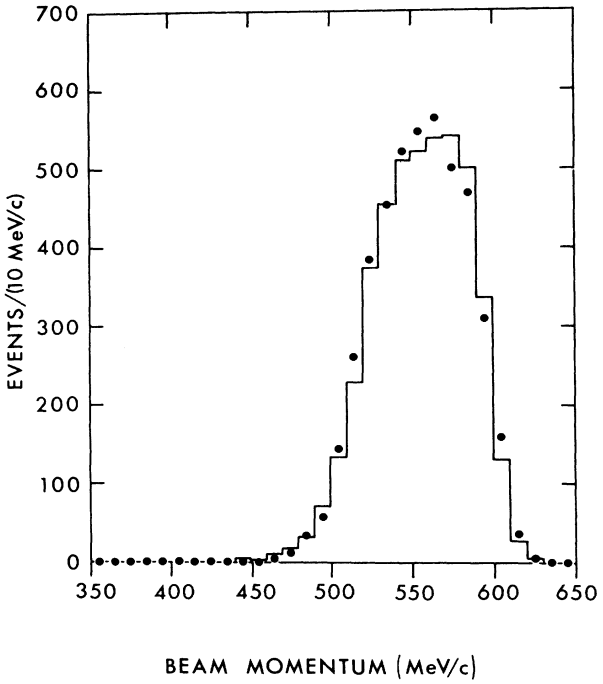

FIG. 2. Beam momentum spectrum. The histogram gives the measured momentum distribution as derived from the reactions $K_L^0 p \to \Lambda\pi^+$ and $K_L^0 p \to K_S^0 p$. The dots are the values obtained for the Monte Carlo calculation, as described in the text.

the muon mass hypothesis, was longer than the muon range as calculated from the track curvature.

About 45 000 events were reconstructed within the fiducial volume and kinematically constrained using the program SQUAW. Since the beam momentum vector is known, we were able to perform one-constraint fits to the following decay hypotheses:

$$K_L^0 \to \pi^+\pi^-\pi^0, \tag{7a}$$

$$K_L^0 \to \pi^\pm e^\mp \nu, \tag{7b}$$

$$K_L^0 \to \pi^\pm \mu^\mp \nu. \tag{7c}$$

SQUAW was set to pass any hypothesis with a χ^2 probability, $P(\chi^2)$, greater than 0.1%. After remeasurement, more than 95% of the K_L^0 decay candidates passed reconstruction and fitting; the remaining events were mainly attributed to K_L^0's which scattered before decaying.

In addition to three-body decays the observed vee candidates could also be due to $K_L^0 p$ interactions.[6] These interactions are easily separated from K_L^0 decays by the kinematic fits. The highly constrained reactions $K_L^0 p \to K_S^0 p$ and $K_L^0 p \to \Lambda^0\pi^+$ proved useful for several purposes. They have been used to check the K_L^0 angular resolution and give the K_L^0 momentum spectrum shown in Fig. 2. In addition these events were also used to estimate the number of K_L^0 which scattered before interaction or decay (10.0± 1.0)%.

III. SELECTION OF THE K_{e3} DATA SAMPLE

Events which had a unique kinematic fit and for which the visual track information, recorded by the scanner, agreed with that fit, were classified accordingly. Kinematically ambiguous events were examined by experienced editors and the visual and measured track information was used to resolve many of the ambiguities. Assuming the previously measured branching ratios for charged K_L^0 decay,[2] the fraction of tracks identified by visual information is given in Table I for K_{e3} decays. The difference in identification between positive and negative pions is expected since in this range of momentum the cross section for πp scattering is larger for positive pions.

This set of K_{e3}^0 candidates was subjected to several tests based on the results of kinematic fitting. The fitted K_L^0 direction had to be consistent with a K_L^0 originating in the hydrogen target. The fitted K_L^0 momentum was required to be in the range

$$-110 \text{ MeV}/c \leq p_{K_L^0}(\text{fit}) - p_{K_L^0}(\text{nominal}) \leq 70 \text{ MeV}/c,$$

where $p_{K_L^0}(\text{nominal})$ was set equal to the mean beam momentum. These limits were determined from the study of the beam characteristics. The beam momentum is sufficiently well known to always yield a single solution for the kinematic fit. Next, a χ^2-ratio criterion was applied: $P(\chi^2)_{K_{e3}^0} \geq 10P(\chi^2)_{\text{other}}$ where $P(\chi^2)_{\text{other}}$ refers to the χ^2 probability of any hypothesis different from the assumed K_{e3} decay mode. After these tests less than 0.5% of the K_{e3}^0 candidates also fit the $K_{3\pi}$ decay hypothesis. These events were assumed to be $K_{3\pi}^0$ if $(P_0')^2 > -6\times10^3$ (MeV/c)^2, where P_0' is the transverse-momentum variable defined in Ref. 5. Otherwise the $K_{3\pi}$ hypothesis was discarded.

This procedure yielded about 21 000 K_{e3}^0 can-

TABLE I. Visual track identification.

Decay mode	Particle identification	Data	Monte Carlo
$K_L^0 \to \pi^+ e^- \bar{\nu}$	π^+	65%	65%
	e^-	51%	50%
$K_L^0 \to \pi^- e^+ \nu$	π^-	50%	51%
	e^+	50%	50%

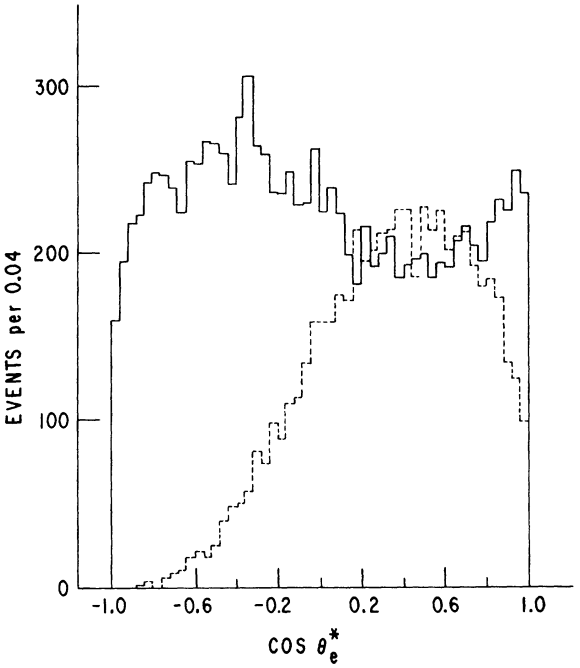

FIG. 3. Distribution of events as a function of $\cos\theta_e^*$. The solid line refers to unique K_{e3}^0 events while the dashed line to events which also fit $K_{\mu 3}$ decay.

didates of which 13 767 events had a unique fit to $K_L^0 \to \pi^+ e^- \nu$ or $K_L^0 \to \pi^- e^+ \nu$. The ambiguous candidates fit one or both of the hypotheses $K_L^0 \to \pi^\mp \mu^\pm \nu$ in addition to the K_{e3}^0 hypothesis. Most of these ambiguous events are decays in which the lepton comes forward with respect to the K_L^0 direction, resulting in a relatively high laboratory momentum and therefore a smaller chance of being identified. The distinction between unique and ambiguous K_{e3} candidates is illustrated in Fig. 3. The solid histogram shows the distribution in $\cos\theta_e^*$ for unique events, where θ_e^* is the angle between the electron and K_L^0 lines of flight in the K_L^0 rest frame. The dashed histogram is the distribution of $\cos\theta^*$ for the ambiguous events. For an unbiased data sample the distribution in $\cos\theta_e^*$ must be flat. The depletion of unique K_{e3}^0 events near $\cos\theta_e^* = -1$ is due to a scanning bias against low-energy electrons and will be discussed below. The unique K_{e3}^0 events also show a depletion near $\cos\theta_e^* = 0.5$, which is a result of our kinematic cuts and is fully reproduced in a Monte Carlo calculation. Since only a minor fraction of the ambiguous events is needed to fill that dip, we conclude that most of the ambiguous events are $K_{\mu 3}^0$ decays (as is borne out by the Monte Carlo calculations). For this reason, only unique K_{e3}^0 events were considered for subsequent analysis.

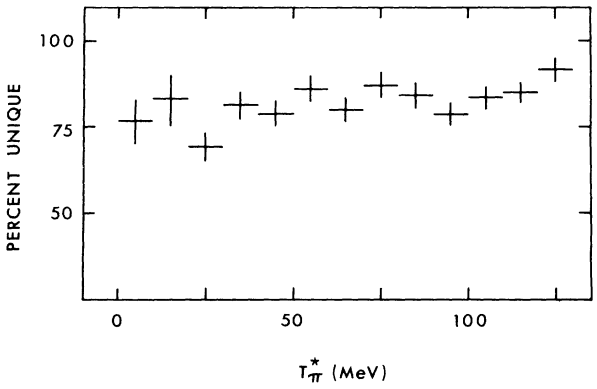

FIG. 4. Percentage of unique K_{e3} events as a function of T_π^*. The percentage of unique K_{e3} events has been corrected for ambiguities as described in the text.

The effect of this selection of unique K_{e3}^0 events has been studied as a function of T_π^*. Since the variables $\cos\theta_e^*$ and T_π^* are independent of each other, the data were divided into bins of T_π^*, and the fraction of the ambiguous events needed to produce a uniform distribution in $\cos\theta_e^*$ was determined for each bin. The result, expressed as the ratio of unique K_{e3}^0 to total K_{e3}^0 events, is shown in Fig. 4. Final corrections for the selection of unique events have been made using a Monte Carlo simulation. But we note that this correction does not seriously depend on the Monte Carlo calculation, since, as shown in Fig. 4 the fraction of unique K_{e3} events is independent of T_π^* within our statistical precision.

IV. CORRECTIONS FOR SCANNING AND RECONSTRUCTION LOSSES

The scanning efficiency for the raw sample of unique K_{e3}^0 events was found to be 83%. However, for some small ranges of laboratory angles and momenta of the charged tracks, the efficiency is considerably smaller than this average. To minimize the variation of efficiency vs the center-of-mass energies, we have imposed cuts based on laboratory quantities to exclude the obviously biased regions.

Events in which the pion interacts or decays close to the K_L^0 decay vertex are difficult to find in the scan and have poorly measured pion tracks. Therefore events with pion track lengths less than 8 cm have been removed and the remaining events have been weighted by the probability that the pion would interact or decay within this distance. Very low momentum tracks and tracks which are nearly parallel to the magnetic field are also likely to be lost in the scanning or reconstruction. This effect has been studied by transforming the events to

the K_L^0 rest frame, rotating each to a random new orientation and transforming back to the laboratory frame. Comparison of the original and randomized data led to the following requirements: for pions, $p_\pi^{lab} \geq 70$ MeV/c $|\lambda_\pi^{lab}| \leq 75°$; and for electrons, $p_e^{lab} \geq 50$ MeV/c, $|\lambda_e^{lab}| \leq 60°$.

The correction for these cuts has been applied in two alternative ways which give identical results. In the first method, a Monte Carlo event sample was subjected to the same cuts as the data and the ratio of Monte Carlo and experimental event densities was analyzed to extract the form factors. The second method utilizes the fact that the laboratory momentum and dip cuts correspond to a restriction on the angular phase space of the K_L^0 decay in its rest frame. This relationship is illustrated in Fig. 5 for a 550-MeV/c K_L^0. The axes are components of laboratory momentum parallel and perpendicular to the K_L^0 direction. The pion kinematics is displayed on the right side of the figure and the electron on the left. The solid lines show the laboratory momentum-angle relationship for fixed center-of-mass energies. The dashed lines correspond to constant values of $\cos\theta^*$, where $\cos\theta^*$ is the angle in the center of mass between the particle and the K_L^0 direction. The shaded areas illustrate the region excluded by the laboratory momentum cuts. Since the center-of-mass kinetic energies are known for each event, the minimum laboratory momentum corresponds to a minimum $\cos\theta^*$ that an event with those energies could have, and the maximum dip to a maximum angle of rotation about the K_L^0 direction. The cuts can therefore be corrected by calculating a weight proportional to the inverse of the angular phase space available for each event. Note that all values of T_π^* are included in the cut data, but the range of $T_e^* \lesssim 20$ MeV is excluded.

The cuts and corresponding correction factors are summarized in Table II. The cut data sample consists of 12 061 $\pi^\pm e^\mp \nu$ events having a ratio

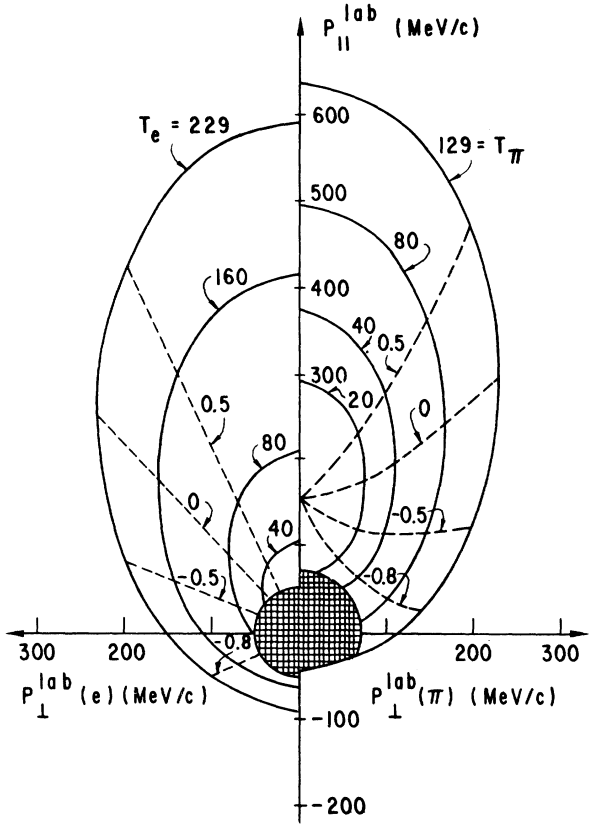

FIG. 5. Kinematics of $K_L^0 \to \pi e \nu$ decay for $P_{lab}(K^0) = 550$ MeV/c. The axes are components of laboratory momentum parallel and transverse to the K_L^0. The solid lines refer to fixed values of kinetic energy in the K_L^0 rest frame. The dashed lines refer to fixed c.m. cosine. The pion kinematics is displayed on the right side of the figure and the electron kinematics is on the left.

$\Gamma_{\pi^- e^+ \nu}/\Gamma_{\pi^+ e^- \nu} = 0.981 \pm 0.018$.

The scanning efficiency for the cut and weighted data sample is shown as a function of the c.m. kinetic energies in Fig. 6. With the exception of

TABLE II. Summary of weights.

Cut	Removed by cut	Average weight
$l_\pi > 8$ cm	120	1.014
$\lvert\lambda_\pi\rvert < 75°, \lvert\lambda_e\rvert < 60°$	836	1.089
$p_\pi > 70$ Mev/c, $P_e > 50$ Mev/c	792	1.076
$T_e^* > 40$ Mev/c	283	
All	1706[a]	1.205

[a]Since some events are removed by more than one cut, the last number is less than the sum of the cuts.

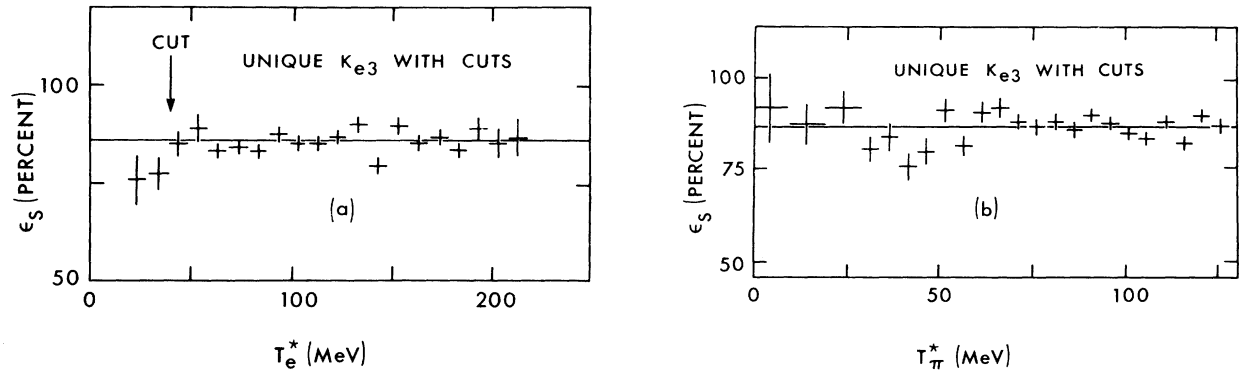

FIG. 6. Scanning efficiency of the cut and weighted data sample as a function of (a) T_e^*, (b) T_π^*.

the region of low-energy electrons mentioned above, this efficiency is independent of the Dalitz-plot coordinates. Hence only the corner of the Dalitz plot with $T_e^* < 40$ MeV is excluded from further analysis.

Since two measurement passes were made we can estimate the measurement and reconstruction efficiency as a function of the Dalitz-plot variables. This efficiency is given approximately by

$$\epsilon_M = 1 - (1 - \epsilon_1)^2 , \tag{8}$$

where ϵ_1 is the ratio of the numbers of events after one and two measurements. Figure 7 shows that this efficiency, which averages (97.0± 0.1)%, is also independent of the center-of-mass kinetic energies.

V. MONTE CARLO SIMULATIONS

We have performed a Monte Carlo simulation of the experiment using a modified version of the program FAKE.[7] The purpose of this calculation was to study in detail the effects of our geometric and kinematic cuts and in particular to estimate and correct for various remaining backgrounds in the selected data sample.

The K_L^0 beam was generated according to the known momentum distribution and spot size of the pion beam, the kinematics of the reaction $\pi^- p \to \Lambda K^0$, and the geometry of the neutral beam. The π^- energy loss in the liquid hydrogen target was the dominant cause of most of the K_L^0 beam momentum spread. Only K_L^0's passing through the bubble-chamber entrance window and decaying within the fiducial volume were accepted. The resultant K_L^0 beam spectrum was found to be in excellent agreement with the spectrum determined from an analysis of the reactions $K_L^0 p \to \Lambda \pi^+$ and $K_L^0 p \to K_S^0 p$, as shown in Fig. 2.

K_{e3}^0 events were generated assuming a pure vector interaction with $\lambda_+ = 0$ and transformed into the laboratory system. The fate of each of the outgoing tracks was determined by propagating the particle through liquid hydrogen until it hit the chamber boundary, interacted, decayed, or was trapped inside the chamber. The following

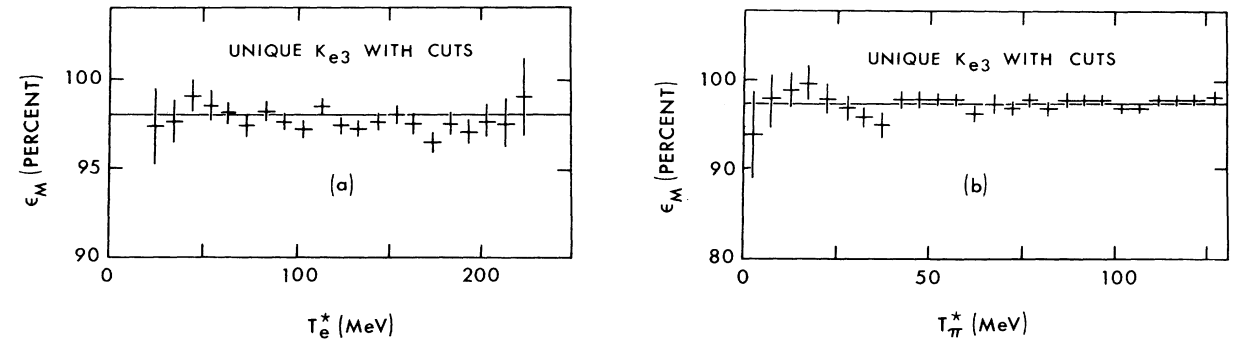

FIG. 7. Measurement and reconstruction efficiency as a function of (a) T_e^*, (b) T_π^*.

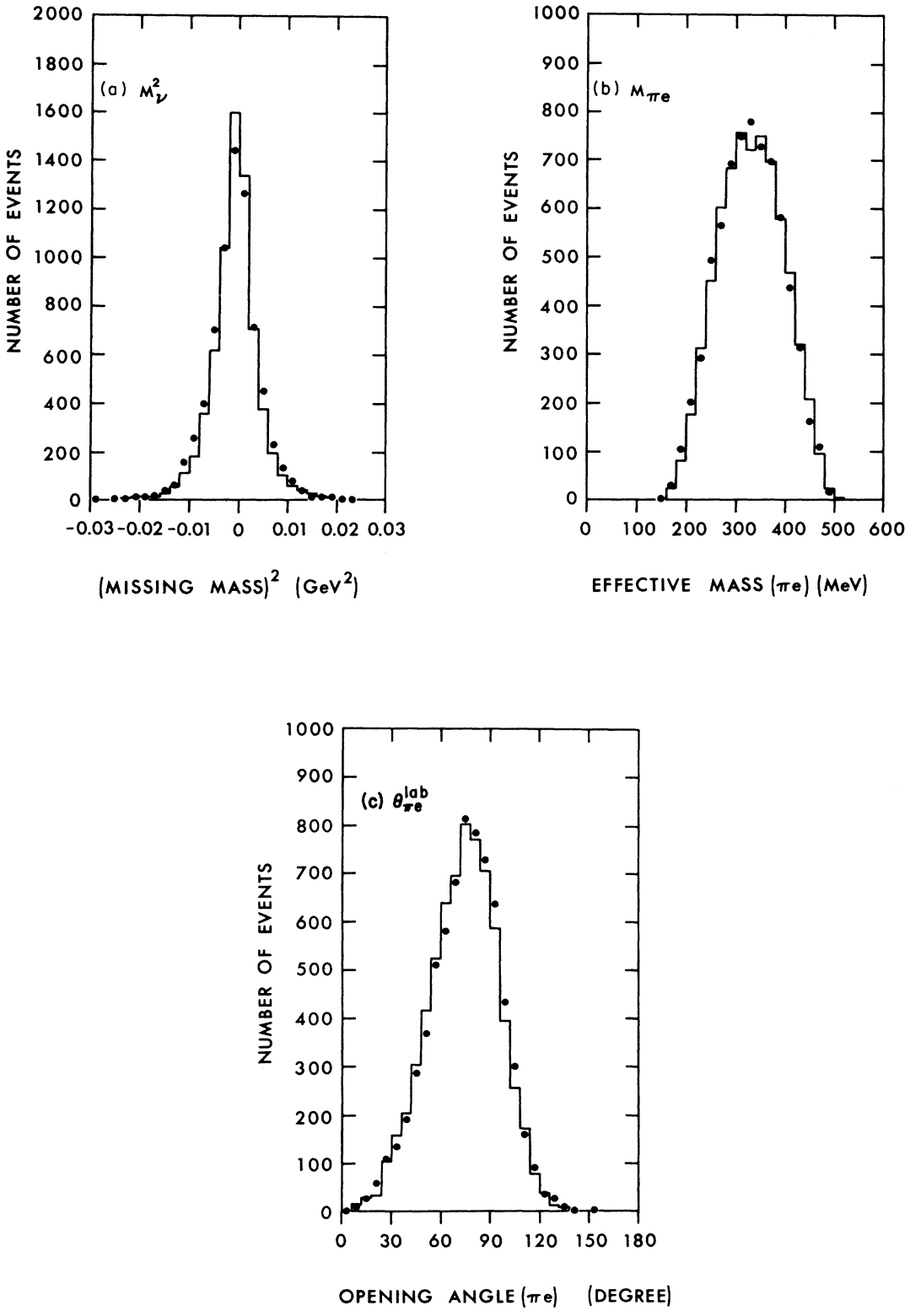

FIG. 8. Comparison of various experimental distributions (solid histograms) with the Monte Carlo–generated distributions (dots): (a) (missing mass)^2 for the neutrino; (b) effective mass of π–e system; (c) laboratory opening angle between π and e, $\theta_{\pi e}^{lab}$.

factors were considered: (1) chamber geometry, (2) variation of the magnetic field, (3) energy loss in liquid hydrogen including radiation loss for electrons, (4) $\pi^{\pm}p$ interactions using the known differential cross sections, (5) decay in flight of π mesons.

The generated tracks were assigned length- and momentum-dependent errors. Particular attention was paid to this procedure since the resolution of ambiguous fits is sensitive to the error assignments. The generated events were then processed through the same kinematic programs and subjected to the same cuts as the real data. The number of generated K^0_{e3} events which survived cuts and fitted the K^0_{e3} decay hypothesis uniquely was approximately twice as large as the data sample.

In comparing the unique K^0_{e3} decays from our Monte Carlo simulation with the data, we first note that for the simulated events the charge asymmetry is $\Gamma_{\pi^-e^+\nu}/\Gamma_{\pi^+e^-\nu} = 0.978 \pm 0.012$, in excellent agreement with the data. In Table I the predicted fraction of tracks identified visually (i.e., by interaction, decay, or trapping) is compared with the data. The validity of the Monte Carlo simulation was further checked by comparing a large number of distributions of the data with the Monte Carlo predictions. The agreement was good, as can be seen from the examples shown in Fig. 8. In addition, most distributions are rather insensitive to the form factor. The acceptance across the Dalitz plot of Monte Carlo events which give a unique K^0_{e3} fit, subject to the cuts mentioned in the previous section, is displayed in Fig. 9.

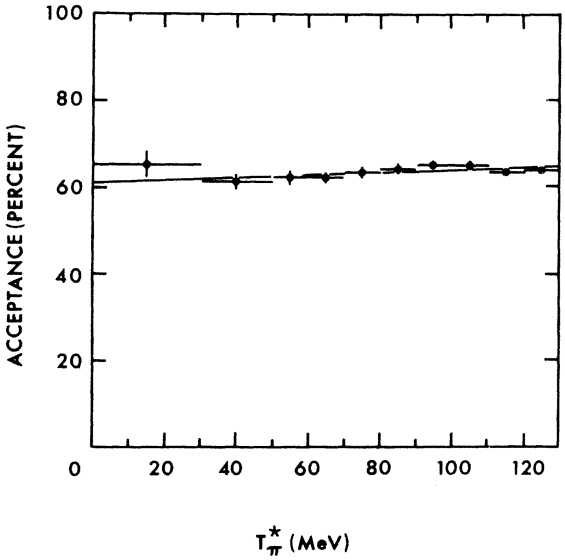

FIG. 9. Acceptance of unique, cut, and weighted Monte Carlo events as function of T^*_π.

$K^0_{\mu 3}$ events were also generated, with $\lambda_+ = 0.03$ and $\xi = f^-(0)/f^+(0) = 0$, and subjected to the same selection criteria as the data. Using the known branching ratios[2] we find that the K^0_{e3} sample contains a contamination of $(5.3 \pm 0.5)\%$ due to $K^0_{\mu 3}$ decay. This contamination is subtracted in the analysis. We find from Monte Carlo calculations that the $K^0_{3\pi}$ contamination in the K^0_{e3} sample is less than 0.05% and we ignore it.

The Monte Carlo calculation also shows that about 0.6% of the selected K^0_{e3} events had the pion and electron identification reversed. Since this occurs for high values of T_e^*, a correction for this interchange has been made. Finally, we generated a sample of K^0_{e3} decays using the parameters of the scattered K^0_L's as determined from the strong interactions. We find that the fraction of these events which would be included in our K^0_{e3} data is $(3 \pm 0.5)\%$. Since there is no statistically significant difference in the Dalitz-plot distribution between events from scattered and unscattered K^0_L's, no corrections for scattered K^0_L's were made.

VI. ANALYSIS AND RESULTS

Since the acceptance is reasonably uniform across the Dalitz plot (in particular there is little dependence on q^2) we expect that a fit to the raw data sample of 13 767 unique events, without corrections for scanning or reconstruction losses or contamination, will yield a result which will only be slightly modified when all corrections are included. Assuming a linear q^2 dependence for $f_+(q^2)$ and using the maximum-likelihood method with the *raw data* sample of unique events, we obtain

$$\lambda_+ = 0.034 \pm 0.003 . \tag{9a}$$

We next apply the cuts summarized in Table II and after the appropriate weighting of the remaining 12 061 events we find $\lambda_+ = 0.031 \pm 0.003$. After a correction for $K_{\mu 3}$ contamination, as given by the Monte Carlo calculation, the result is $\lambda_+ = 0.025 \pm 0.004$. Finally, the cut data sample of 12 061 events, weighted for cuts and corrected for $K_{\mu 3}$ contamination was also corrected for the small variation of the acceptance with q^2, as determined from our Monte Carlo simulation. We obtain the final result,

$$\lambda_+ = 0.028 \pm 0.004 , \tag{9b}$$

including all corrections, except for radiative effects. A second method for determining λ_+ consists of calculating the quantities

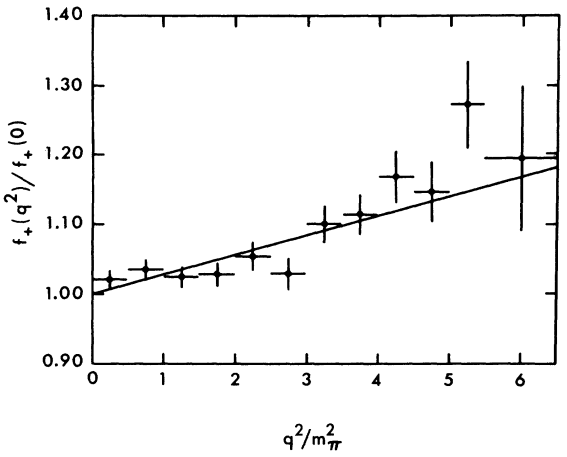

FIG. 10. $f_+(q^2)/f_+(0)$ as a function of q^2. The straight line is the best fit assuming a linear q^2 dependence.

$$\frac{f_+(q^2)}{f_+(0)} \propto \left[\frac{N_{\text{data}}(q^2)}{N_{\text{MC}}(q^2, \lambda_+ = 0)}\right]^{1/2}, \tag{10}$$

where $N_{\text{data}}(q^2)$ is the number of K^0_{e3} events in a given q^2 bin after corrections for $K^0_{\mu 3}$ contamination, and $N_{\text{MC}}(q^2)$ is the number of Monte Carlo events in the same q^2 bin, subjected to the same cuts and normalized to the data at $q^2 = 0$. The values of $f^+(q^2)/f^+(0)$ are plotted in Fig. 10. Assuming a linear q^2 dependence, a least-squares fit gives

$$\lambda_+ = 0.028 \pm 0.005, \tag{9c}$$

with $\chi^2/\text{DF} = 15.4/10$ corresponding to a probability $P(\chi^2) = 12\%$. If the data are fitted to the form

$$f_+(q^2)/f_+(0) = 1 + \lambda'_+(q^2/m_\pi^2) + \lambda''_+(q^2/m_\pi^2)^2,$$

the result is $\lambda'_+ = -0.016 \pm 0.015$, $\lambda''_+ = 0.010 \pm 0.003$, with $P(\chi^2) = 72\%$. Since a linear fit is satisfactory, we shall restrict our further discussion to that case.

All errors quoted are statistical, including the contribution from the weighting and the statistical errors on the Monte Carlo sample. However, the values for λ_+ after all corrections are taken into account, (9b), differ by about one standard deviation from the value obtained from the uncorrected data sample of unique events, (9a). We thus believe that the effect of the systematic error is small compared to the statistical error quoted.

TABLE III. Radiative corrections.

T_π^* (Mev)	Δ_{RC}
20–40	0.00 ± 0.05
40–60	0.00 ± 0.04
60–80	-0.03 ± 0.03
80–100	-0.02 ± 0.03
100–120	0.01 ± 0.02
> 120	-0.01 ± 0.03

To obtain an estimate of the effect of radiative corrections, we compare the shape of the observed energy spectrum for electrons with that predicted by the vector interaction (i.e., the Monte Carlo prediction without radiative corrections). Following Gjesdal *et al.*[4] we define the fractional deviation

$$\Delta_{\text{RC}} = \frac{N_{\text{exp}}(T_e^*) - N_{\text{MC}}(T_e^*)}{N_{\text{MC}}(T_e^*)}, \tag{11}$$

where $N_{\text{exp}}(T_e^*)$ is the observed distribution of events, and $N_{\text{MC}}(T_e^*)$ is the same distribution for an equal number of Monte Carlo events. Table III shows the average of Δ_{RC} for several T_π^* bins. The measured deviations are consistent with zero. Within our statistical accuracy we also find no dependence of Δ_{RC} on T_e^*, for given T_π^* bins, indicating that the radiative corrections are expected to be small. Using the calculation of Ginsberg[8] we obtain

$$\lambda_+ = 0.025 \pm 0.005. \tag{9d}$$

VII. CONCLUSIONS

The 1976 world average[2] of λ_+ values obtained from K^0_{e3} experiments was $\lambda_+ = 0.0288 \pm 0.0028$. However, the consistency among the early experiments is not satisfactory. Table IV shows the results from recently reported high-statistics

TABLE IV. Comparison of recent K^0_{e3} decay experiments.

	No. of Events	λ_+
Blumenthal (Ref. 9)	25 000	0.0270 ± 0.0028
Buchanan (Ref. 10)	24 000	0.044 ± 0.006
Gjesdal (Ref. 4)	500 000	0.0312 ± 0.0012
This experiment	12 000	0.025 ± 0.005

experiments.[4,9,10] With the possible exception of the experiment of Buchanan *et al.*,[10] the results are mutually consistent and in agreement with the assumption of $K^*(890)$ dominance. Since the world average[2] for K_e^+ is $\lambda_+^+ = 0.0285 \pm 0.0043$, the $\Delta I = \frac{1}{2}$ rule appears well satisfied. Finally, we note that the λ_+ value of 0.0314 ± 0.0027 as determined from $K_{\mu 3}^0$ experiments, which are dominated by the high-statistics experiment of Donaldson *et al.*,[3] is also in good agreement with the K_{e3}^0 measurements, and thus supports μe universality.

ACKNOWLEDGMENTS

We wish to express our thanks to the staffs of the Zero Gradient Synchrotron and the 12-ft bubble chamber who made this experiment possible. We also thank our scanning and measuring staff for their painstaking efforts. Finally, we thank Drs. H. E. Fisk, L. G. Hyman, and J. S. Russ for their help during the early part of this experiment. This work was supported in part by the U. S. Department of Energy.

---

*Present address: General Electric Medical Systems Division, Milwaukee, Wi. 53201.

†Present address: Brookhaven National Lab., Upton, L. I., New York 11973. This work was submitted in partial fulfillment of the Ph.D. requirement at Carnegie-Mellon University.

‡Present address: Tel-Aviv University, Tel-Aviv, Israel.

[1]L. M. Chounet, J. M. Gaillard, and M. K. Gaillard, Phys. Rep. 4C, 199 (1972).

[2]Particle Data Group, Rev. Mod. Phys. 48, S72 (1976).

[3]G. Donaldson *et al.*, Phys. Rev. D 9, 2960 (1977).

[4]G. Gjesdal *et al.*, Nucl. Phys. B109, 118 (1976).

[5]Y. Cho *et al.*, Phys. Rev. D 15, 587 (1977).

[6]Y. Cho *et al.*, Phys. Lett. 60B, 293 (1976); J. Schlereth, Ph.D. thesis, Carnegie-Mellon University, 1977 (unpublished).

[7]G. Lynch, Report No. UCRL 10335 and CERN Track Chamber Program Library, 1967 (unpublished).

[8]E. S. Ginsberg, Phys. Rev. 171, 1675 (1968); 174, 269 (1968).

[9]R. Blumenthal *et al.*, Phys. Rev. Lett. 34, 114 (1975).

[10]C. D. Buchanan *et al.*, Phys. Rev. D 11, 457 (1975).

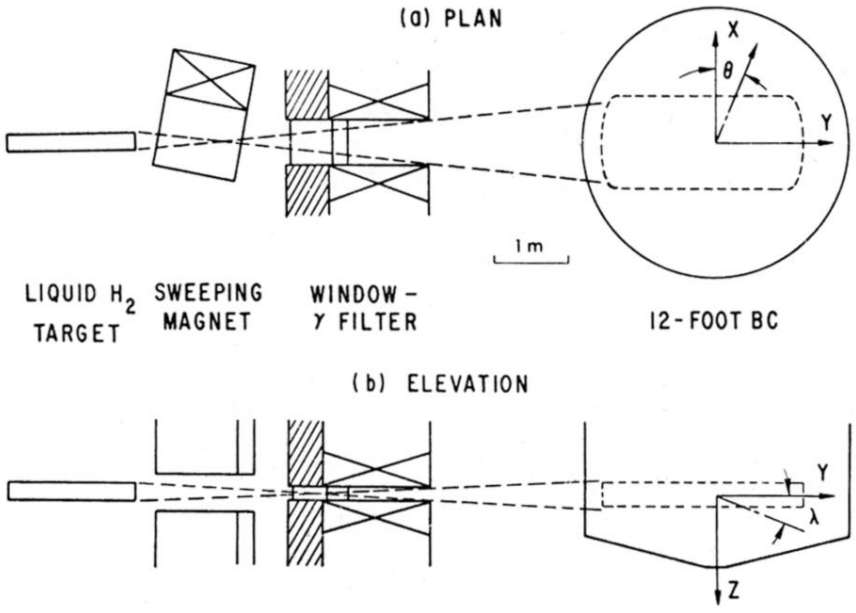

FIG. 1. End section of the beam, showing schematically the relationship between the target, the K_L^0 window, and the bubble chamber. The chamber fiducial volume is also indicated.

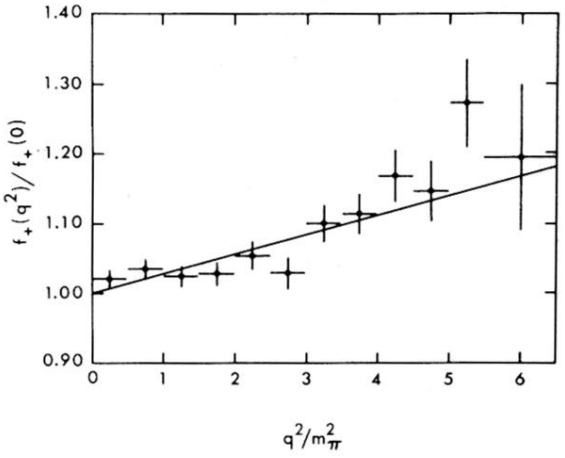

FIG. 10. $f_+(q^2)/f_+(0)$ as a function of q^2. The straight line is the best fit assuming a linear q^2 dependence.

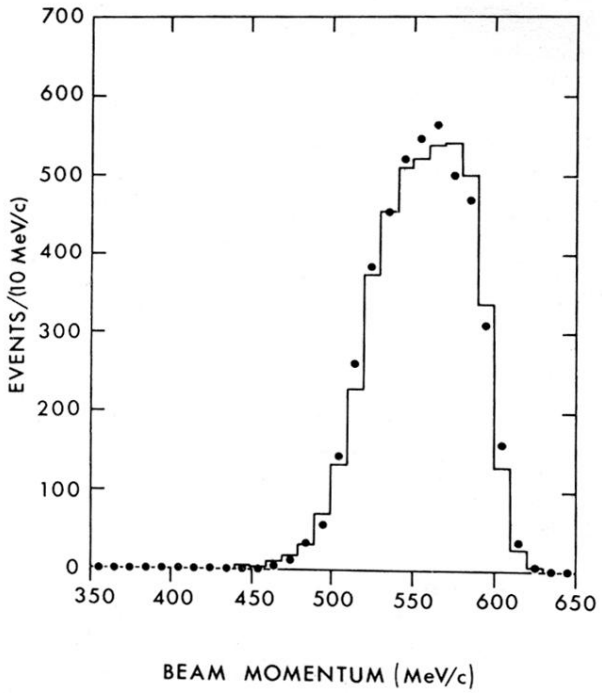

FIG. 2. Beam momentum spectrum. The histogram gives the measured momentum distribution as derived from the reactions $K_L^0 p \rightarrow \Lambda\pi^+$ and $K_L^0 p \rightarrow K_S^0 p$. The dots are the values obtained for the Monte Carlo calculation, as described in the text.

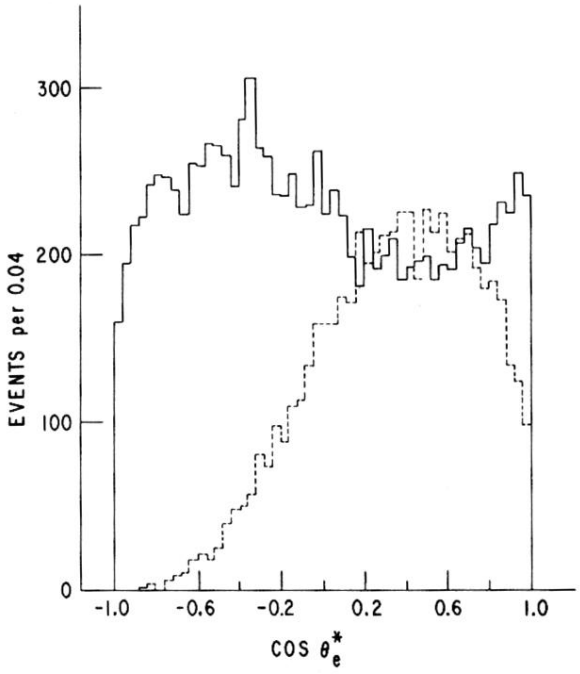

FIG. 3. Distribution of events as a function of $\cos\theta_e^*$. The solid line refers to unique K_{e3}^0 events while the dashed line to events which also fit $K_{\mu 3}$ decay.

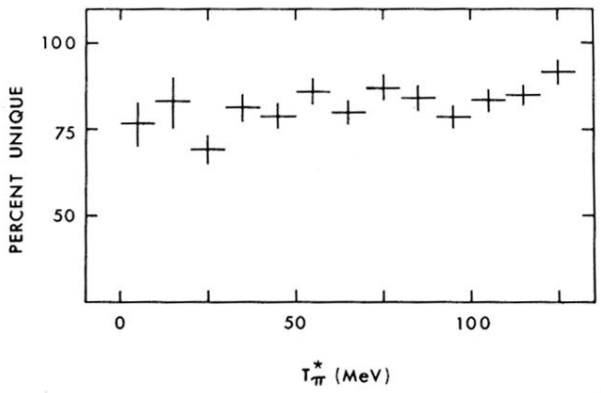

FIG. 4. Percentage of unique K_{e3} events as a function of T_π^*. The percentage of unique K_{e3} events has been corrected for ambiguities as described in the text.

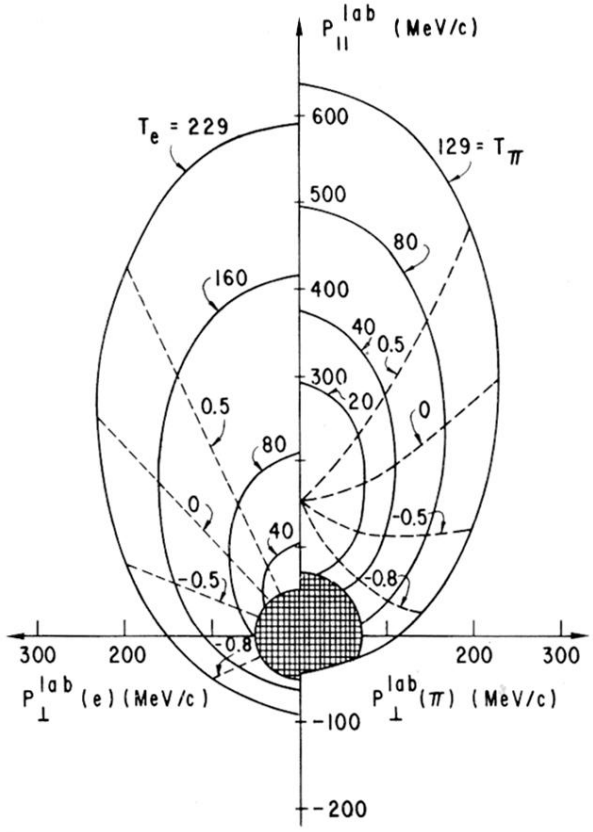

FIG. 5. Kinematics of $K_L^0 \rightarrow \pi e \nu$ decay for $P_{lab}(K^0) = 550$ MeV/c. The axes are components of laboratory momentum parallel and transverse to the K_L^0. The solid lines refer to fixed values of kinetic energy in the K_L^0 rest frame. The dashed lines refer to fixed c.m. cosine. The pion kinematics is displayed on the right side of the figure and the electron kinematics is on the left.

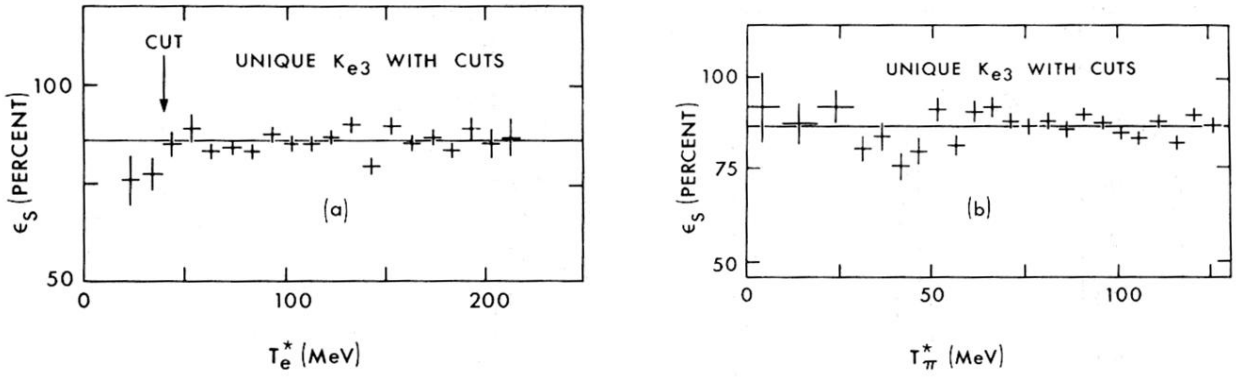

FIG. 6. Scanning efficiency of the cut and weighted data sample as a function of (a) T_e^*, (b) T_π^*.

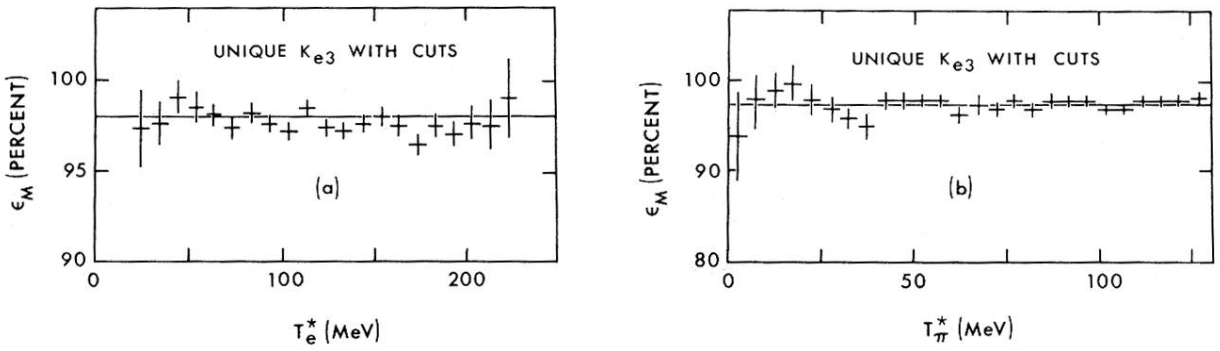

FIG. 7. Measurement and reconstruction efficiency as a function of (a) T_e^*, (b) T_π^*.

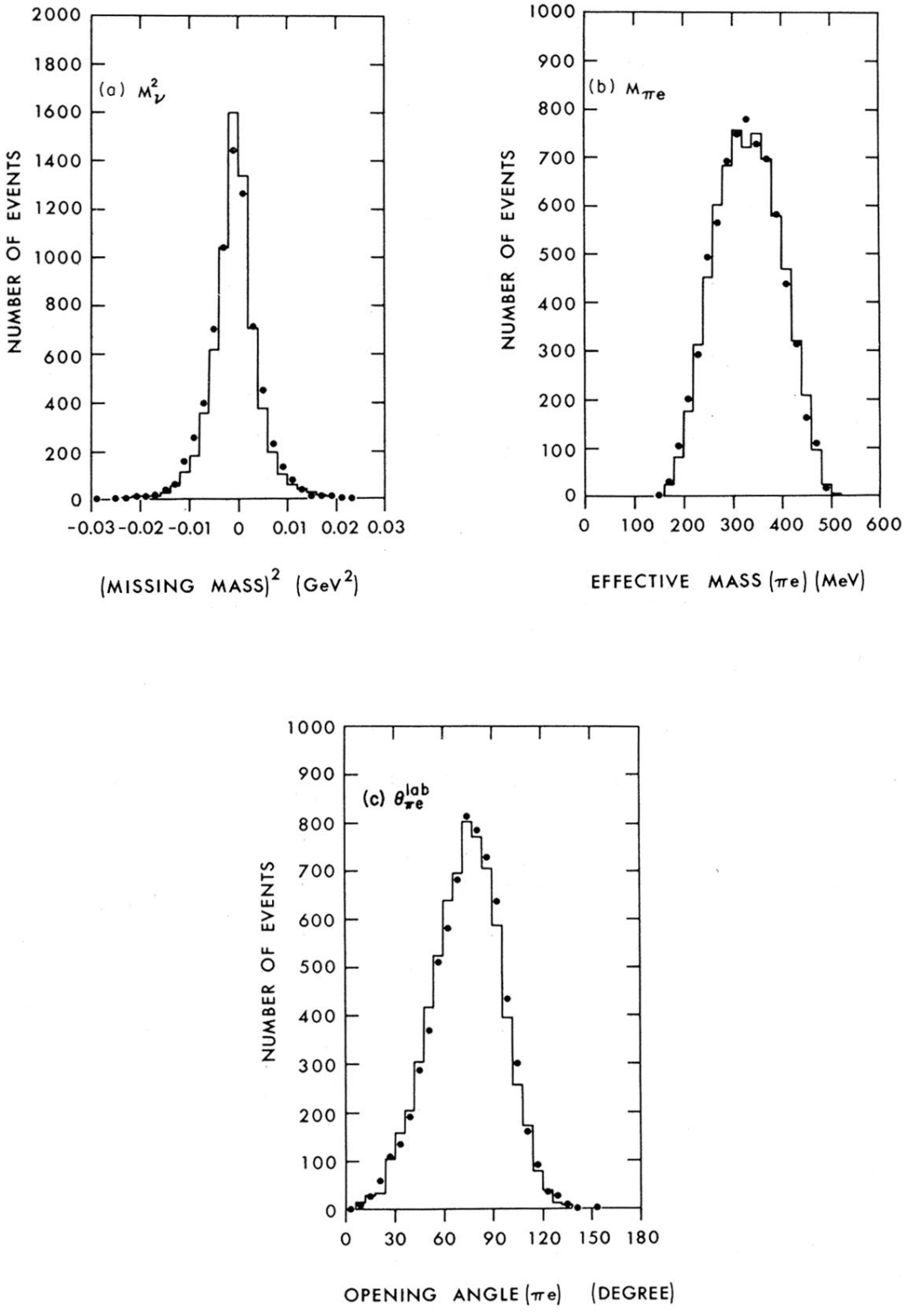

FIG. 8. Comparison of various experimental distributions (solid histograms) with the Monte Carlo–generated distributions (dots): (a) (missing mass)^2 for the neutrino; (b) effective mass of π–e system; (c) laboratory opening angle between π and e, $\theta_{\pi e}^{lab}$.

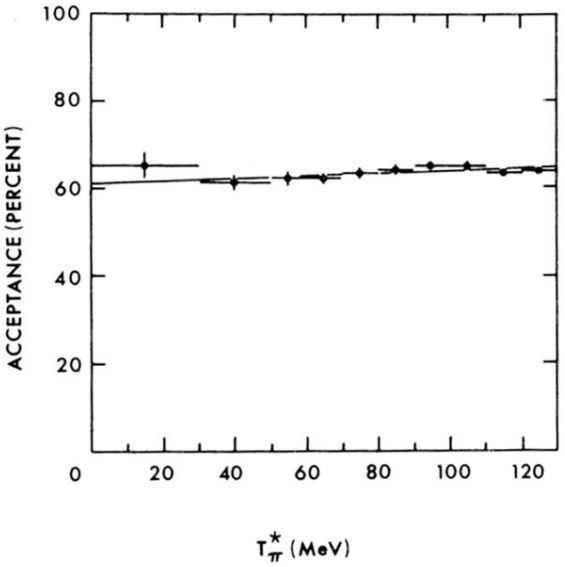

FIG. 9. Acceptance of unique, cut, and weighted Monte Carlo events as function of T_π^*.